JACS
JOURNAL OF THE AMERICAN CHEMICAL SOCIETY

ARTICLE

pubs.acs.org/JACS

In Situ Oxidation Study of Pt(110) and Its Interaction with CO

Derek R. Butcher,[†,#,$] Michael E. Grass,[†,‡,#] Zhenhua Zeng,[§] Funda Aksoy,[†,∥] Hendrik Bluhm,[†] Wei-Xue Li,[*,§] Bongjin S. Mun,[*,‡] Gabor A. Somorjai,[†,⊥] and Zhi Liu[*,†]

[†]Lawrence Berkeley National Laboratory, Berkeley, California 94720, United States

[‡]Department of Applied Physics, Hanyang University, ERICA, Korea 426-791

[§]State Key Laboratory of Catalysis, Dalian Institute of Chemical Physics, Chinese Academy of Sciences, Dalian 116023, People's Republic of China

[∥]Department of Physics, Faculty of Arts and Sciences, Nigde University, Nigde, Turkey

[⊥]Department of Chemistry, University of California, Berkeley, California 94720, United States

Supporting Information

ABSTRACT:

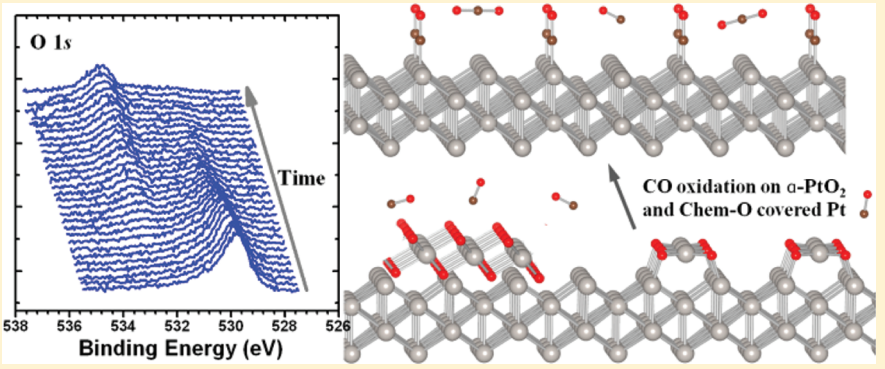

Many interesting structures have been observed for O_2-exposed Pt(110). These structures, along with their stability and reactivity toward CO, provide insights into catalytic processes on open Pt surfaces, which have similarities to Pt nanoparticle catalysts. In this study, we present results from ambient-pressure X-ray photoelectron spectroscopy, high-pressure scanning tunneling microscopy, and density functional theory calculations. At low oxygen pressure, only chemisorbed oxygen is observed on the Pt(110) surface. At higher pressure (0.5 Torr of O_2), nanometer-sized islands of multilayered α-PtO_2-like surface oxide form along with chemisorbed oxygen. Both chemisorbed oxygen and the surface oxide are removed in the presence of CO, and the rate of disappearance of the surface oxide is close to that of the chemisorbed oxygen at 270 K. The spectroscopic features of the surface oxide are similar to the oxide observed on Pt nanoparticles of a similar size, which provides us an extra incentive to revisit some single-crystal model catalyst surfaces under elevated pressure using in situ tools.

INTRODUCTION

CO oxidation on transition-metal surfaces is one of the most thoroughly investigated systems in heterogeneous catalysis, due to its importance in automotive exhaust treatment and water-gas shift as well as its ability to shed light on fundamental catalyst properties.[1,2] In particular, the study of CO oxidation on Pt(110) has received much attention over the last two decades. Self-sustained oscillations and spatiotemporal patterns form on this surface[3−6] as well as a variety of surface oxides.[7,8] Furthermore, there is still an ongoing debate regarding the influence of surface structure on CO oxidation kinetics.[8,9] To fully understand and model these fascinating phenomena, we need further in situ characterization of adsorbed oxygen and oxide phases of Pt(110) in O_2 and CO and under reaction conditions.

Newly developed in situ surface characterization techniques have led to many recent results concerning CO oxidation on Pt(110). These include ambient-pressure X-ray photoelectron spectroscopy (AP-XPS),[10−12] high-pressure scanning tunneling microscopy (HP-STM),[8] surface X-ray diffraction,[13] and polarization modulation infrared reflection absorption spectroscopy.[14] These new results have provided new insights into whether there is oxide formation during the reaction and whether this oxide is responsible for "superior reactivity", though no consensus has been reached.[8,9,14]

In a previous AP-XPS investigation of CO oxidation on Pt(110), we established that the surface is either covered with chemisorbed CO or chemisorbed O depending on the reaction conditions, with no evidence for a surface oxide under any conditions investigated.[12] Herein, we used AP-XPS, HP-STM,

Received: August 2, 2011
Published: November 08, 2011

ACS Publications © 2011 American Chemical Society

and density functional theory (DFT) calculations to investigate the oxidation of Pt(110) at different temperatures and pressures of pure O_2. Our AP-XPS results show that two different oxygen-related species form on Pt(110) at 0.5 Torr of oxygen pressure. One belongs to an island-structured surface oxide that forms under elevated pressure. The other belongs to chemisorbed oxygen, which has been commonly observed in UHV experiments. HP-STM images under similar conditions confirm the formation of these oxide islands. The identification of the surface oxide species is supported by DFT calculations. CO titration experiments on the oxidized Pt(110) surface demonstrate that both chemisorbed oxygen and the surface oxide react with gas-phase CO at 270 K at similar rates.

Although no consensus has been reached on the CO oxidation mechanism at high O_2/CO ratios, there is agreement regarding the dramatic changes in surface morphology of these metal surfaces at elevated pressure. Surface reconstruction at elevated pressure often leads to the formation of nanometer-sized features that do not form under the low P_{O_2} conditions of typical UHV experiments.[7,15,16] Such changes will not affect the bulk properties of the material. They will, however, dramatically modify the surface properties of material, which are crucial in many important applications (such as catalysts, battery/fuel cell electrodes, ...). Furthermore, as the sizes of components decrease to the nanometer scale, surface properties play increasingly important roles in determining the properties. For instance, in electronic devices and interconnects, changes to the metal surfaces under real conditions can even affect some traditional bulk properties such as electron transport (due to the change of surface scattering and electronic structure). Therefore, it is important for researchers to understand how these reconstructions can change the morphology and electronic structure of metal surfaces. We believe these observations provide an opportunity to investigate nanoparticle catalysts and other nanoscale phenomena. The formation of surface oxide islands may build a bridge between single crystals and nanoparticle catalysts. Interestingly, we found that the XPS chemical shift of the Pt 4f peak from the nanostructured Pt(110) surface oxide is similar to that of the Pt oxide peak observed on Pt nanoparticles of similar size (1.5 nm).

EXPERIMENTAL SECTION

AP-XPS experiments were performed at Beamlines 11.0.2 and 9.3.2 at the Advanced Light Source. Both endstations consist of an analysis and a preparation chamber. Detailed descriptions of the AP-XPS endstations used in this study can be found in previous reports.[17,18] The HP-STM experiments were performed on a UHV system with a chamber for single-crystal preparation and characterization and a smaller HP-STM chamber.[19] A Pt(110) single crystal from Matek, polished on both sides, was used in this study. The sample cleaning process included repeated cycles of Ar^+ sputtering and oxygen annealing and a final annealing at 1000 K under vacuum in the sample preparation chamber. The clean sample was transferred under vacuum to the analysis chamber where in situ experiments were performed. The surface was checked with XPS or AES to confirm the absence of contaminants.

Self-consistent total energy DFT calculations on various oxygen-covered and CO-covered Pt(110) and Pt oxide surfaces were performed using the Vienna ab initio simulation package (VASP) with projector augmented wave potentials and generalized gradient approximation in the Perdew–Burke–Ernzerhof formalism for the exchange-correlation functional.[20,21] A cutoff energy of 400 eV was used for the plane-wave expansion for all calculations. Optimized bulk lattice constants were used throughout the present work: a = 3.98 Å for fcc Pt; a = 3.15 Å, c = 4.03 Å for α-PtO_2; a = 4.61 Å, b = 4.55 Å, c = 3.19 Å for β-PtO_2; a = 4.58 Å, c = 3.29 Å for rutile PtO_2. The Pt(110)-(1 × 2) missing row, reconstructed Pt(110)-(12 × 2)-22O chemisorption structure, α-PtO_2-(0001)-(2 × 2), β-PtO_2(110)-(2 × 1), and rutile-PtO_2(110)-(2 × 1) surfaces (Figure 1) were used to simulate various surface structures. The core-level binding energy shifts were calculated including final state effects. The details used in these calculations have been reported previously.[22]

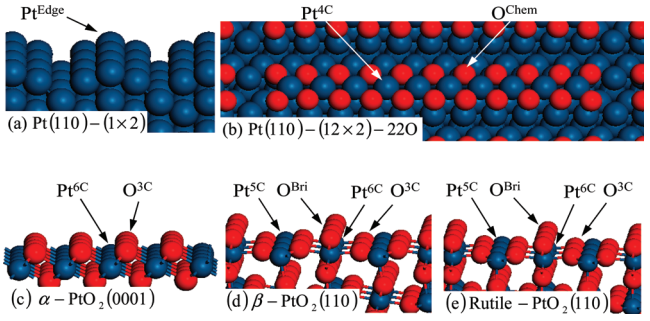

Figure 1. Schematic structures for (a) metal Pt(110)-(1 × 2) missing row, (b) Pt(110)-(12 × 2)-22O chemisorption, (c) α-PtO_2(0001), (d) β-PtO_2(110), and (e) rutile-PtO_2(110) surfaces used for DFT calculations. The different Pt (blue) and O (red) species are indicated.

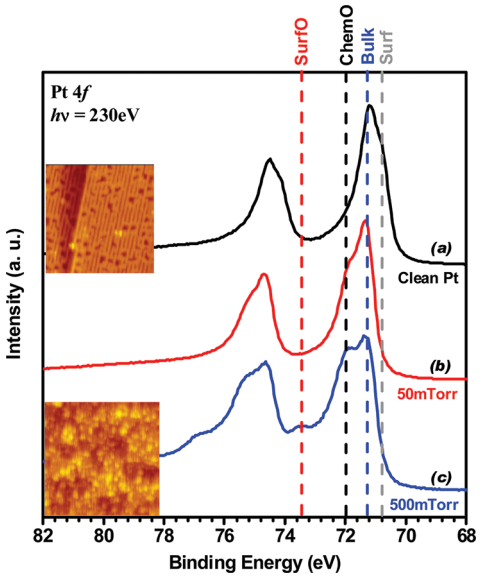

Figure 2. (a) The Pt 4f spectrum taken after sputtering and annealing in UHV is composed of a peak from bulk Pt at 71.2 eV and a surface peak at lower binding energy (70.8 eV, CLS = −0.4 eV). (b) Under 0.05 Torr of O_2 an additional peak at 71.9 eV (CLS = 0.7 eV) appears. This peak corresponds to surface Pt atoms bonded to the oxygen atom. (c) When the O_2 pressure is increased to 0.5 Torr, a third peak at 73.4 eV is observed, corresponding to the formation of a surface oxide. STM images taken under similar conditions (clean surface and under 0.2 Torr of O_2 at 423 K) are shown as inserts. The high-pressure image shows a roughened surface with nanometer islands (see the Supporting Information for additional STM data).

RESULTS AND DISCUSSION

To study the oxidation of Pt(110) under elevated oxygen pressure, we exposed a clean Pt(110) surface to increasing O_2 pressure while monitoring the Pt 4f, O 1s, and C 1s core level

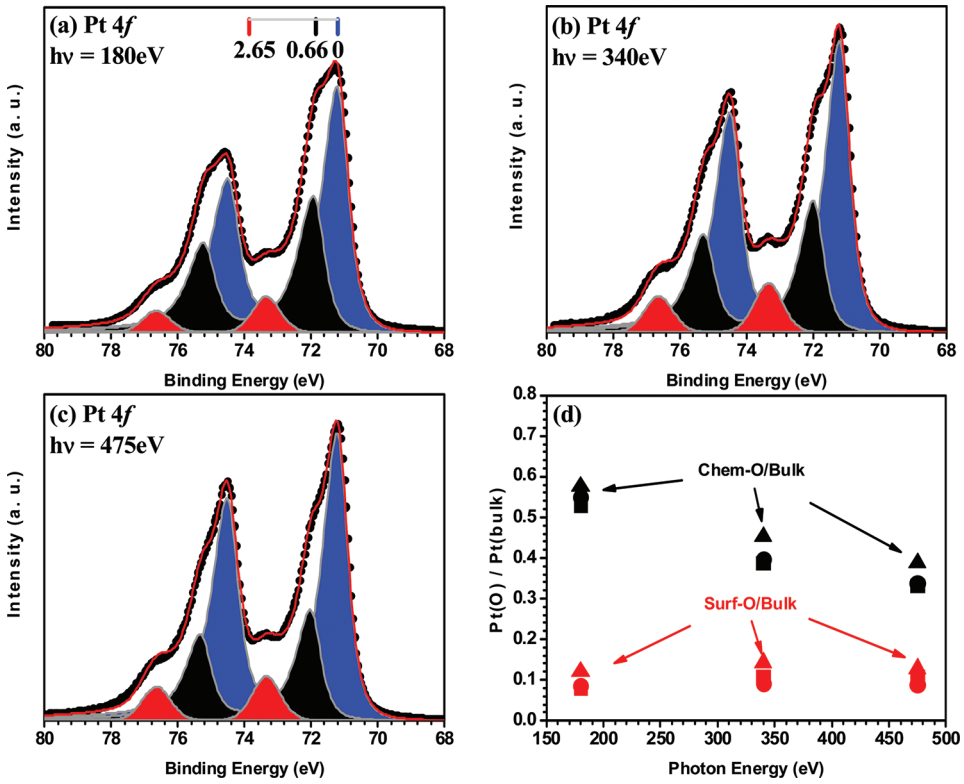

Figure 3. Pt 4f spectra obtained at 180, 340, and 475 eV under 0.5 Torr of O_2 at 473 K are shown in (a), (b), and (c) respectively. We fit the spectra with two oxygen induced Pt 4f doublets in addition to the bulk Pt 4f peak (blue). These peaks arise from Pt atoms chemisorbed to oxygen (black) and the surface oxide (red). (d). The intensity ratios of Pt(Chem-O)/Pt(bulk) and Pt(Surf-Ox)/Pt(bulk) are plotted as a function of photon energy. The symbols ■, ●, and▲ represent data obtained at 300, 373, and 473 K, respectively. The Pt(Chem-O) intensity decreases with increasing photon energy, while the Pt(Surf-O) peak intensity remains constant. The calculated Pt 4f shift of reconstructed chemisorption and α-PtO_2(0001) with respect to bulk are indicated in (a).

peaks. The Pt $4f_{7/2}$ region for clean Pt(110) can be fitted with two peaks (Figure 2a, 230 eV photon energy), corresponding to bulk Pt (71.2 ± 0.1 eV) and surface Pt with a surface core level shift (CLS) of −0.4 eV (70.8 ± 0.1 eV).[23] The surface peak arises from under-coordinated Pt atoms in the topmost atomic layer, indicating a clean surface. This was confirmed by the absence of any spectral features other than Pt peaks. In a separate experiment using the same single crystal, the clean surface was characterized using STM (Figure 2a insert and Figure S-1 (Supporting Information)). The image shows flat terraces separated by single-atom steps. The terraces have parallel rows resulting from the (1 × 2) missing row reconstruction. There are also point defects of oxygen atoms, which appear as depressions in STM images.[24]

The Pt 4f surface CLS changes from −0.4 to +0.7 eV after 10^{-8} Torr of O_2 exposure, corresponding to surface Pt atoms bonded to chemisorbed oxygen atoms. Increasing the pressure to 0.05 Torr of O_2 leads to an increase in the intensity of the Pt 4f peak at 71.9 eV from Pt surface atoms bound to chemisorbed oxygen (Chem-O). This Chem-O shoulder is well-resolved from the bulk Pt 4f peak at 71.2 eV (Figure 2b). There is also a slight intensity increase on the high-binding-energy (BE) side of the Chem-O peak. Increasing the pressure to 0.5 Torr further increases the Chem-O peak intensity relative to that of the bulk Pt peak and a third peak at 73.4 eV arises, which is assigned to a surface oxide (Surf-O) (Figure 2c). Under these conditions, there are two peaks in the O 1s region: a peak at 529.7 eV corresponding to Chem-O and a high-BE shoulder at 530.8 eV that we ascribe to the Surf-O (Figure S-2, Supporting Information). Similar Pt 4f spectra were also obtained at 373 and 473 K (Figure 3). STM images at 0.2 Torr of O_2 and 423 K indicate a roughened surface with 1 nm lateral features that are 0.2 nm in apparent height (Figure 2c insert and Figure S-1), which is in agreement with previous STM experiments up to 1 atm of O_2[8] or after atomic oxygen exposure.[7] The surface oxide forms upon exposure to an elevated pressure of oxygen in the absence of the X-ray beam but increases dramatically upon high-intensity X-ray exposure (see the Supporting Information). Once formed, the Surf-O is stable at low pressure and remains on the surface after evacuating to UHV.

The formation of surface oxide distinct from chemisorbed oxygen has been claimed by numerous reports on various Pt surfaces, especially on Pt(111), using XPS. Some early reports were found to be associated with Si or Ca impurities in the Pt crystals.[25−27] To our knowledge, fewer such claims have been made for Pt(110).[28,29] A Pt 4f peak with a BE very similar to our current report was observed by Bonzel et al.[28] after exposing a Pt(110) surface to atomic oxygen, but no identification was provided. A recent STM and temperature-programmed desorption study on the Pt(110) surface[7] reported nanostructured island formation after atomic oxygen or high-pressure molecular oxygen exposure. With the help of DFT calculations, the authors associated these islands with patches of a surface oxide phase. In that study, a reconstructed Pt(110)-(12 × 2)-2O chemisorption

Table 1. Calculated Pt 4f and O 1s CLSs (eV) on Various Clean, Reconstructed, Chemisorption and Oxide Surfaces[a]

	Pt 4f CLS (eV)	O 1s CLS (eV)
Pt(110)-(1 × 2)	−0.42 (Pt^{Edge})	
Pt(110)-(12 × 2)-2O	0.66 (Pt^{4C})	−2.40 to −2.60 (O^{Chem})
α-PtO_2(0001)-(2 × 2)	2.65 (Pt^{6C})	−1.80 (O^{3C})
β-PtO_2(110)-(2 × 1)	2.25 (Pt^{6C})	−3.98 (O^{Bri})
	1.20 (Pt^{5C})	−2.32 (O^{3C})
rutile PtO_2(110)-(2 × 1)	2.15 (Pt^{6C})	−4.02 (O^{Bri})
	1.15 (Pt^{5C})	−2.39 (O^{3C})

[a] The energy references are metallic bulk Pt and O 1s of on-top CO on the Pt(110)-(1 × 2) surface.

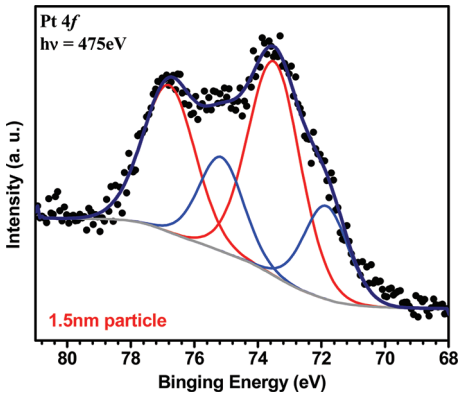

Figure 4. Pt 4f spectrum of 1.5 nm Pt nanoparticles as synthesized. The Pt 4f region is fit with two doublets assigned to a reduced Pt peak at 71.9 eV and an oxidized Pt peak at 73.4 eV.

structure was found and is assigned to the Chem-O phase in the present work.

To identify the nature of the peak at 73.4 eV, Pt 4f spectra were collected at photon energies of 180, 340, and 475 eV in the presence of 0.5 Torr of O_2 (Figure 3). Since the inelastic mean free path of photoelectrons increases with kinetic energy in the energy range of these experiments, decreasing the photon energy causes the spectra to be more sensitive to the topmost surface layer. The spectra in Figure 3 had a Shirley background subtracted and were fitted with an asymmetric Voigt profile.[30] The fitting was performed with three doublet peaks: bulk Pt (71.2 eV), Pt bound to chemisorbed oxygen (71.9 eV), and Pt in the surface oxide phase (73.4 eV), where the BE refers to that of Pt $4f_{7/2}$. At photon energies of 180, 340, and 475 eV, the Pt 4f photoelectrons have inelastic mean free paths of 4, 6, and 7 Å, respectively.[31] As the photon energy increased from 180 to 475 eV, the relative area of the Chem-O induced Pt 4f peak decreased with respect to the bulk Pt 4f peak while that of the surface oxygen phase remained constant. The relative areas measured at 300, 373, and 473 K are plotted in Figure 3d. The decrease in relative peak area of Pt bound to Chem-O with increasing energy is expected, since these atoms are only found in the surface layer. The Surf-O peak, however, does not decrease appreciably with photon energy, indicating that it is a subsurface phase.

The peak at 73.4 eV clearly corresponds not to Pt atoms coordinated to Chem-O atoms but those located below the surface. For simplicity, we refer to it as a Surf-O following ref 7. From the intensity ratio of the Surf-O and Chem-O peaks, we estimate the coverage of the surface oxide to be 0.15 ML at 0.5 Torr. On the basis of our STM and XPS results, we conclude that the nanometer-sized islands observed in this and previous studies[7] are a surface oxide associated with a multilayer (≥2) of PtO_x. This surface oxide is stable at 473 K under vacuum and completely decomposes by 573 K. The formation of this surface oxide was also found to be defect dependent, forming more readily on surfaces prepared with a short final annealing step, which increases the step edge density. These observations are consistent with the results in ref 7.

To elucidate the structure and reactivity of such a surface oxide, we calculated Pt 4f and O 1s (Table 1) core level shifts for a clean Pt surface (Pt(110)-(1 × 2)missing row), a Pt surface bound to chemisorbed oxygen (Pt(110)-(12 × 2)-2O), and three bulk Pt oxide structures (α-PtO_2(0001)-(2 × 2), β-PtO_2-(110)-(2 × 1), and rutile PtO_2(110)-(2 × 1)) using DFT. The oxide structures contain Pt atoms coordinated to five and six oxygen atoms (Pt^{5C} and Pt^{6C}). In comparison to bulk metallic Pt, the Pt 4f CLSs for the six-oxygen coordinated surface (Pt^{6C}) for α-PtO_2(0001)-(2 × 2), β-PtO_2(110)-(2 × 1), and rutile PtO_2-(110) are 2.65, 2.25, and 2.15 eV, respectively. The five-oxygen coordinated surface (Pt^{5C}) 4f CLSs are 1.20 and 1.15 eV for β-PtO_2(110)-(2 × 1) and rutile PtO_2(110)-(2 × 1), respectively. We also calculated Pt 4f CLSs of the clean metallic surface: Pt(110)-(1 × 2) (Pt^{Edge}), the oxygen chemisorbed surface Pt(110)-(12 × 2)-2O (Pt^{4C}), and the CO covered surface Pt(110)-(1 × 2) with on-top CO. These CLSs are −0.42, 0.66, and 0.95 eV, respectively. The calculated Pt^{4C} 4f CLS (0.66 eV) for Pt(110)-(12 × 2)-2O agrees well with our measured chemisorbed oxygen related Pt 4f peak at 71.9 eV (0.70 eV CLS).

For all three oxides considered, the O 1s CLSs were also calculated for both bridging oxygen (O^{Bri}) and oxygen coordinated to three platinum atoms (O^{3C}) and referenced to the O 1s peak of CO at an on-top site on the Pt(110) surface. The O 1s CLSs of β-PtO_2 and rutile PtO_2 are −3.98 and −4.02 eV for O^{Bri} and −2.32 and −2.39 eV for O^{3C}, which are large compared to the CLSs of experimentally measured surface oxide shifts −2.9 ± 0.2 and −1.8 ± 0.2 eV, respectively (Figure 5). The absence of a peak at a CLS of −4 eV is a clear evidence that β-PtO_2 and rutile PtO_2 are not consistent with the experimental data. This can safely rule out β-PtO_2 and rutile PtO_2 as the majority phase of the observed surface oxide. Therefore, we assign the surface oxide to a structure similar to α-PtO_2. The difference in the Pt 4f CLSs between the calculated Pt^{6C} for the α-PtO_2 and the measured Pt 4f of the surface oxide (2.65 vs 2.2 ± 0.1 eV) could be attributed to the role of the metal support or particle size effect of the surface oxide islands, which are not considered in the calculation. As the surface oxide grows, the BE of the Surf-O peak shifts from 73.4 to 73.6 eV (see the Supporting Information). Thus, the CLS of the Surf-O peak increases from 2.2 eV to 2.4 eV, approaching the calculated value of 2.65 eV. As the nanoscale oxide islands grow, the metal support and particle size effects of the surface oxide islands become less significant. This also may explain that the CLS values measured here are smaller than the bulk oxide values measured before.[32] Such α-PtO_2-like nanoscale surface oxide islands may have electronic and chemical properties different from those of the bulk α-PtO_2, which is assumed to be inert to CO. The present XPS measurements and calculations corroborate previous STM and DFT studies,[7] in which the nanoscale islands were proposed to be α-PtO_2-like in character.

We have confirmed the formation of nanometer-sized surface oxide islands on Pt(110) at elevated oxygen pressure. These

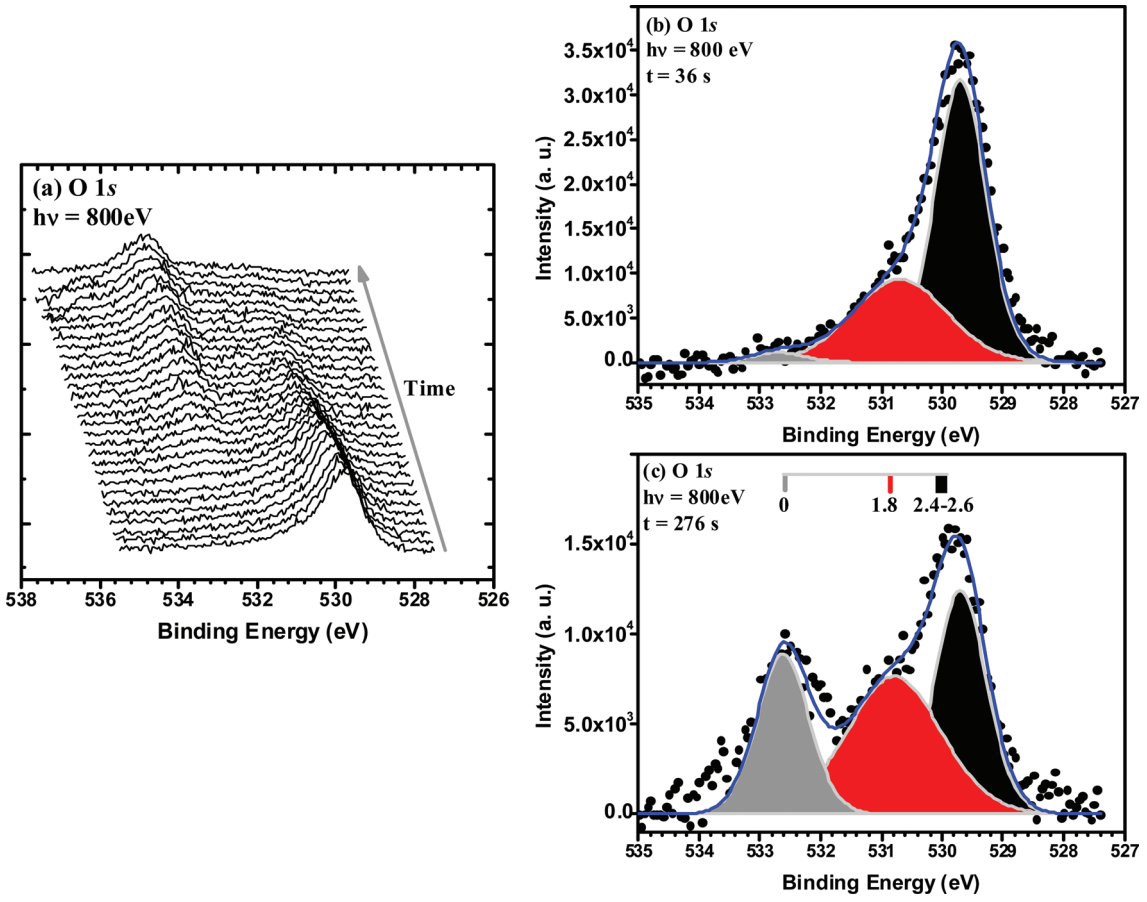

Figure 5. (a) O 1s spectra recorded every 12 s from the O-covered Pt(110) surface in the presence of 10^{-6} Torr CO. (b, c) Selected O 1s spectra taken at t = 36 and 276 s after dosing CO into the chamber. Calculated O 1s shifts of reconstructed chemisorption and α-PtO_2(0001) with respect to on-top CO on Pt(110) are indicated in (c). Please note the scale difference of the vertical axes in (b) and (c).

islands are similar in size to catalytically relevant Pt nanoparticles. An interesting question is whether there is a connection between these oxide islands on Pt(110) and the oxide on catalytically relevant Pt nanoparticles. As-prepared Pt nanoparticles have often been found in oxidized form (see the Supporting Information). It has been shown that the dissociation pressure of oxide thin films and nanoparticles can be several orders of magnitude lower than for the same bulk material.[33,34]

In Figure 4, we show the Pt 4f spectrum of as-prepared solution-phase synthesized 1.5 nm monodispersed platinum nanoparticles with a poly(vinylpyrrolidone) capping.[35] The monolayer films of particles were then prepared in a Langmuir–Blodgett trough. The spectrum was fit with two Pt 4f doublets and a Shirley background. Unlike the Pt 4f peak fitting on the Pt(110) surface, we used a symmetric Voigt line shape here to reflect the difference in final state effects between bulk and nanoparticles.[36] The BE values of the two Pt $4f_{7/2}$ peaks are 71.9 and 73.4 eV. It has been suggested that the 73.4 eV peak belongs to Pt oxide[37] or a peak induced by the capping of Pt NPs.[38] Unlike the dendrimer samples used in refs 37 and 38, the nanoparticles used here were prepared through a different method and different capping. This indicates that the similarity in XPS peaks is less likely due to the capping layer. Therefore, we assign the higher energy peak to the Pt oxide; its BE is identical with the surface oxide island peak we observed on Pt(110). This indicates that the surface oxide formed under high-pressure oxygen exposure is similar to the NP oxide. The formation of surface oxide islands under near-ambient conditions observed here and in previous studies suggests a link between single crystals and nanoparticle catalysts. This provides additional motivation to revisit single-crystal surfaces at elevated pressure. The 71.9 eV peak has the same BE as a Chem-O peak. It is likely to result from Pt atoms coordinated to less than six oxygen atoms, which is similar to Chem-O. We would like to point out that the smaller Pt clusters can have higher BE than that of bulk metallic Pt as shown in ref 36.

The similarity between the surface oxide islands on Pt(110) and the oxide on Pt nanoparticles motivated us to evaluate the reactivity of different oxygen species on Pt(110) toward identifying reactive oxygen species in nanoparticle catalysis. We checked the reactivity toward CO oxidation by exposing the nanometer sized surface oxide on Pt(110) to a low pressure of CO (10^{-6} Torr) at 270 and 275 K while monitoring with continuous fast XPS scans. In this CO titration study we investigate the oxide layer within the limits of the pressure and time constraints of ambient-pressure XPS. As has been shown in previous work, the oxide phase rapidly reacts under catalytic conditions for CO oxidation on time scales too short for XPS studies.[8,9,12,14] Due to the limitations in low coverage and short time scales, we have monitored both the formation of the oxide phase in the presence of pure oxygen as well as its removal by CO at a decreased temperature and low pressure, allowing direct in situ characterization by XPS. While this is not the optimal regime for the active

Table 2. Reaction Rates Measured for O 1s Peaks at 270 and 275 K[a]

	270 K		275 K	
	529.7 eV Chem-O	530.8 eV Surf-O	529.7 eV Chem-O	530.8 eV Surf-O
linear fit	3.1	1.9	5.7	3.9
fit to model	3.2	1.8	6.2	3.9

[a] Rates given in $\times 10^{-3}$ s^{-1}.

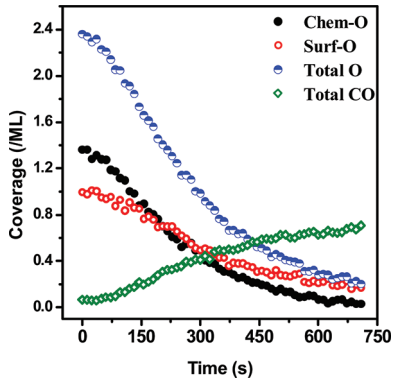

Figure 6. O and CO coverage of a Pt(110) surface exposed to 0.5 Torr of O_2 and then exposed to 10^{-6} Torr of CO at 270 K.

catalyst, it does allow direct measurement of the stability and activity of the oxide phase.

The Pt(110) surface containing both chemisorbed and surface oxide species was prepared by exposure to 0.5 Torr of O_2. Although beam damage was negligible during spectroscopy measurements, it was pronounced when we increased the photon flux (see the Supporting Information). This beam-induced oxidation was used to increase the signal-to-noise ratio by preparing a higher initial surface oxide coverage using 230 eV X-rays with an intensity 10 times higher than that used for our aforementioned and subsequent spectroscopy measurements. The surface oxidation induced by the X-ray source and the consequent secondary electrons is likely a result of the defect and kinetic restrictions to surface oxide formation described by Li et al.[7] After the surface oxide had been prepared, the sample was cooled to the titration temperature and O_2 was evacuated from the chamber to a base pressure of $<10^{-9}$ Torr. The reaction between oxygen species and gas-phase CO was performed by introducing 10^{-6} Torr CO at either 270 or 275 K and monitoring the O 1s or Pt 4f signal versus time. We chose these temperatures and CO pressure to ensure the titration experiments were not limited by CO flux, but were sufficiently slow to capture good statistics.

The O 1s spectra taken during the titration are shown in Figure 5a. It takes 12 s to collect each spectrum. The spectra (Figure 5b,c) were fit with three peaks at 529.7 ± 0.2 eV (CLS = −2.9 eV), 530.8 ± 0.2 eV (CLS = −1.8 eV), and 532.6 ± 0.2 eV (CLS = 0 eV), belonging to chemisorbed O, surface oxide, and on-top CO, respectively. These observed CLSs are in good agreement with the DFT calculated values of −2.4 to −2.60 eV (O^{Chem}) for chemisorbed oxygen and −1.8 eV (O^{3C}) for α-PtO_2(0001)-(2 × 2) (Table 1). However, the surface oxide peak has a significantly larger fwhm than the other two peaks. This indicates the surface oxide is less well-defined. This effect may also contribute to the difference that we found between measured and calculated Pt 4f Surf-O CLSs.

We also conducted the CO titration experiment while monitoring the Pt 4f region. The results from these experiments are qualitatively similar. The Pt 4f peaks at +0.66 and +2.65 eV corresponding to Chem-O and Surf-O Pt atoms decrease in intensity with time while a peak measured and calculated at +0.95 eV (Pt coordinated with CO on clean Pt(110) surface) grows in. The two O-coordinated Pt 4f peaks disappear simultaneously, but quantitative fitting is challenging because of the small peak separation between chemisorbed O and chemisorbed CO induced peaks (see the Supporting Information).

On the basis of this peak assignment, we calculated the reaction rate using the disappearance of the O 1s peak at 529.7 ± 0.2 eV (associated primarily with chemisorbed O) and at 530.8 ± 0.2 eV (predominately surface oxide). After the initial period, a linear slope is obtained. A second method is to fit the decay of the O 1s signal to the equation

$$\theta_O = [\theta_O|_{t=t_0}{}^{1-\alpha} - (1-\alpha)k'(t-t_0)]^{1/(1-\alpha)}$$

where θ_O is the oxygen coverage at time t, α is a constant, and

$$k' = cv \exp(-E_a/k_B T)$$

where v is the pre-exponential factor, E_a is the activation energy, c is a geometrical factor describing the size and shape of O islands, k_B is Boltzmann's constant, and T is temperature. We used this equation with α = 0.63 to obtain a second value of the reaction rate at each temperature.[39]

On the basis of the O 1s peak fitting shown in Figure 5b,c, the rates measured at both temperatures are summarized in Table 2. The rate is higher for the chemisorbed oxygen than for the surface oxide in this temperature range, but by less than a factor of 2. The coverage of each O species and adsorbed CO are plotted in Figure 6 for the reaction at 270 K. These results are consistent with previous theoretical calculations,[40,41] in which there are small energy barriers for CO oxidation at the reconstructed Pt-(110)-(12 × 2)-2O surface and at the $(10\bar{1}0)$ facet of α-PtO_2; however, the barrier is large on the perfect α-PtO_2(0001) surface. The rate calculated for chemisorbed oxygen is higher than that calculated for chemisorbed oxygen on Pt(111) by Denecke et al.[39] It is unclear whether O atoms in the α-PtO_2 react directly with CO or if α-PtO_2 destabilized at interfaces with CO covered Pt and O from this phase decomposes into chemisorbed O on neighboring Pt sites. Another possibility is that the α-PtO_2 reacts only at the boundary of α-PtO_2 and metallic Pt.[41]

CONCLUSION

Oxidation of open surfaces of late transition metals leads to a variety of structures, which have been investigated with respect to their reactivity. In this work we have combined AP-XPS, HP-STM, and DFT calculations to demonstrate that the Pt(110) surface reconstructs into a nanostructured surface when it is exposed to an elevated pressure of O_2. This surface contains regions of metallic Pt with chemisorbed oxygen and α-PtO_2 domains that are ≥2 layers thick. Both of these oxygen species react with CO at 273 K and 10^{-6} Torr of CO. The rate of disappearance of chemisorbed O is faster than that of α-PtO_2, but by less than a factor of 2. Finally, the surface oxide formed under high-pressure oxygen exposure is similar to the NP oxide. This

observation provides us an extra incentive to revisit some single-crystal model catalyst surfaces under elevated pressure using in situ tools.

■ ASSOCIATED CONTENT

Supporting Information. Figure S1−S5, giving additional information on DFT calculations, STM images, O 1s spectra at different pressures, dissociation pressure of oxide nanoparticles, X-ray beam induced damage, beam -induced oxidation at high photon flux, and Pt 4f spectra during CO titration experiments. This material is available free of charge via the Internet at http://pubs.acs.org.

■ AUTHOR INFORMATION

Corresponding Author

*E-mail: zliu2@lbl.gov (Z.L.); bsmun@hanyang.ac.kr (B.S.M.); wxli@dicp.ac.cn (W.-X.L.).

Present Addresses

$Department of Chemistry & Chemical Biology, Harvard University, Cambridge, MA 02138.

Author Contributions

#These authors contributed equally.

■ ACKNOWLEDGMENT

The Advanced Light Source is supported by the Director, Office of Science, Office of Basic Energy Sciences, of the U.S. Department of Energy under Contract No. DE-AC02-05CH11231. We thank Dr. Yimin Li for the fruitful discussion. W.-X.L. acknowledges financial support by the National Science Foundation of China (Nos. 20873142 and 20923001), the Ministry of Science and Technology of China (No. 2007CB815205). B.S.M. appreciates the support of the Korea Research Foundation (KRF) grant funded by the Korean government (MEST) (No. 2009-0068720). M.E.G. acknowledges the support of the ALS Postdoctoral Fellowship program.

■ REFERENCES

(1) Ertl, G. *Surf. Sci.* **1994**, *299/300*, 742–754.
(2) Somorjai, G. A. *Introduction to Surface Chemistry and Catalysis*, 1st ed.; Wiley: New York, 1994.
(3) Imbihl, R.; Ertl, G. *Chem. Rev.* **1995**, *95*, 697–733.
(4) Oertzen, A. V.; Mikhailov, A. S.; Rotermund, H. H.; Ertl, G. *J. Phys. Chem. B* **1998**, *102*, 4966–4981.
(5) Oertzen, A. V.; Rotermund, H. H.; Mikhailov, A. S.; Ertl, G. *J. Phys. Chem. B* **2000**, *104*, 3155–3178.
(6) Oertzen, A. V; Mikhailov, A.; Rotermund, H. H.; Ertl, G. *Surf. Sci.* **1996**, *350*, 259–270.
(7) Li, W. X.; Österlund, L.; Vestergaard, E. K.; Vang, R. T.; Matthiesen, J.; Pedersen, T. M.; Lægsgaard, E.; Hammer, B.; Besenbacher, F. *Phys. Rev. Lett.* **2004**, *93*, 146104.
(8) Hendriksen, B. L. M.; Frenken, J. W. M. *Phys. Rev. Lett.* **2002**, *89*, 046101.
(9) Gao, F.; Wang, Y.; Cai, Y.; Goodman, D. W. *J. Phys. Chem. C* **2009**, *113*, 174–181.
(10) Ogletree, D. F.; Bluhm, H.; Lebedev, G.; Fadley, C. S.; Hussain, Z.; Salmeron, M. *Rev. Sci. Instrum.* **2002**, *73*, 3872.
(11) Salmeron, M.; Schlögl, R. *Surf. Sci. Rep.* **2008**, *63*, 169–199.
(12) Chung, J.; Aksoy, F.; Grass, M. E.; Kondoh, H.; Ross, P., Jr.; Liu, Z.; Mun, B. S. *Surf. Sci.* **2009**, *603*, L35–L38.
(13) Ackermann, M. D.; Pedersen, T. M.; Hendriksen, B. L. M.; Robach, O.; Bobaru, S. C.; Popa, I.; Quiros, C.; Kim, H.; Hammer, B.; Ferrer, S.; Frenken, J. W. M. *Phys. Rev. Lett.* **2005**, *95*, 255505.
(14) McClure, S. M.; Goodman, D. W. *Chem. Phys. Lett.* **2009**, *469*, 1–13.
(15) Tao, F.; Dag, S.; Wang, L.; Liu, Z.; Butcher, D. R.; Bluhm, H.; Salmeron, M.; Somorjai, G. A. *Science* **2010**, *327*, 850–853.
(16) Hendriksen, B. L. M.; Ackermann, M. D.; van Rijn, R.; Stoltz, D.; Popa, I.; Balmes, O.; Resta, A.; Wermeille, D.; Felici, R.; Ferrer, S.; FrenkenJoost, W. M. *Nat. Chem.* **2010**, *2*, 730–734.
(17) Ogletree, D. F.; Bluhm, H.; Hebenstreit, E. D.; Salmeron, M. *Nucl. Instrum. Methods Phys. Res., Sect. A* **2009**, *601*, 151–160.
(18) Grass, M. E.; Karlsson, P. G.; Aksoy, F.; Lundqvist, M.; Wannberg, B.; Mun, B. S.; Hussain, Z.; Liu, Z. *Rev. Sci. Instrum.* **2010**, *81*, 053106.
(19) Somorjai, G. A.; York, R. L.; Butcher, D.; Park, J. Y. *Phys. Chem. Chem. Phys.* **2007**, *9*, 3500–3513.
(20) Kresse, G.; Furthmüller, J. *Phys. Rev. B* **1996**, *54*, 11169–11186.
(21) Kresse, G.; Joubert, D. *Phys. Rev. B* **1999**, *59*, 1758–1775.
(22) Zeng, Z. H.; Ma, X. F.; Ding, W. C.; Li, W. X. *Sci. China Chem.* **2010**, *53*, 402–410.
(23) Baetzold, R. C.; Apai, G.; Shustorovich, E.; Jaeger, R. *Phys. Rev. B* **1982**, *26*, 4022–4027.
(24) Robert, V. *J. Phys. Chem. A* **1999**, *103*, 6805–6810.
(25) Bonzel, H.; Franken, A.; Pirug, G. *Surf. Sci.* **1981**, *104*, 625–642.
(26) Niehus, H.; Comsa, G. *Surf. Sci. Lett.* **1980**, *93*, L147–L150.
(27) Niehus, H.; Comsa, G. *Surf. Sci. Lett.* **1981**, *102*, L14–L20.
(28) Dückers, K.; Prince, K. C.; Bonzel, H. P.; Cháb, V.; Horn, K. *Phys. Rev. B* **1987**, *36*, 6292.
(29) Wang, J. G.; Li, W. X.; Borg, M.; Gustafson, J.; Mikkelsen, A.; Pedersen, T. M.; Lundgren, E.; Weissenrieder, J.; Klikovits, J.; Schmid, M.; Hammer, B.; Andersen, J. N. *Phys. Rev. Lett.* **2005**, *95*, 256102.
(30) Fairley, N. Carrick, A. *The Casa Cookbook Part 1*, Acolyte Science: Cheshire, 2005.
(31) Powell, C.; Jablonski, A. *NIST Electron Inelastic-Mean Free-Path Database, Standard Reference Data Program Database 71, Version 1.1*; National Institute of Standards and Technology, Gaithersburg, MD, 2000.
(32) Wagner, C. D.; Naumkin, A. V.; Kraut-Vass, A.; Allison, J. W.; Powell, C. J.; Rumble, J. R.; Wagner, C. D.; Naumkin, A. V.; Kraut-Vass, A.; Allison, J. W.; Powell, C. J.; Rumble, J. R., Jr. *NIST X-ray Photoelectron Spectroscopy Database, version 3.5 (web version)*; National Institute of Standards and Technology, Gaithersburg, MD, 2003.
(33) Campbell, C. T. *Phys. Rev. Lett.* **2006**, *96*, 066106.
(34) Grass, M.; Zhang, Y.; Butcher, D.; Park, J.; Li, Y.; Bluhm, H.; Bratlie, K.; Zhang, T.; Somorjai, G. *Angew. Chem., Int. Ed.* **2008**, *47*, 8893–8896 (supporting materials).
(35) Tsung, C.; Kuhn, J. N.; Huang, W.; Aliaga, C.; Hung, L.; Somorjai, G. A.; Yang, P. *J. Am. Chem. Soc.* **2009**, *131*, 5816–5822.
(36) Eberhardt, W.; Fayet, P.; Cox, D. M.; Fu, Z.; Kaldor, A.; Sherwood, R.; Sondericker, D. *Phys. Rev. Lett.* **1990**, *64*, 780.
(37) Huang, W.; Kuhn, J. N.; Tsung, C.; Zhang, Y.; Habas, S. E.; Yang, P.; Somorjai, G. A. *Nano Lett.* **2008**, *8*, 2027–2034.
(38) Ye, H.; Scott, R. W. J.; Crooks, R. M. *Langmuir* **2004**, *20*, 2915–2920.
(39) Kinne, M.; Fuhrmann, T.; Zhu, J. F.; Whelan, C. M.; Denecke, R.; Steinrück, H. *J. Chem. Phys.* **2004**, *120*, 7113–7122.
(40) Pedersen, T. M.; Li, W. X.; Hammer, B. *Phys. Chem. Chem. Phys.* **2006**, *8*, 1566–1574.
(41) Li, W. X.; Hammer, B. *Chem. Phys. Lett.* **2005**, *409*, 1–7.